AIP Journal of Applied Physics

First-principles study of carbon impurities in CuInSe2 and CuGaSe2, present in non-vacuum synthesis methods

J. Bekaert, R. Saniz, B. Partoens, and D. Lamoen

Citation: Journal of Applied Physics **117**, 015104 (2015); doi: 10.1063/1.4905538
View online: http://dx.doi.org/10.1063/1.4905538
View Table of Contents: http://scitation.aip.org/content/aip/journal/jap/117/1?ver=pdfcov
Published by the AIP Publishing

First-principles study of carbon impurities in $CuInSe_2$ and $CuGaSe_2$, present in non-vacuum synthesis methods

J. Bekaert,[a] R. Saniz, B. Partoens, and D. Lamoen
CMT-Group and EMAT, Department of Physics, University of Antwerp, Groenenborgerlaan 171, B-2020 Antwerp, Belgium

(Received 23 September 2014; accepted 20 December 2014; published online 7 January 2015)

A first-principles study of the structural and electronic properties of carbon impurities in $CuInSe_2$ and $CuGaSe_2$ is presented. Carbon is present in organic molecules in the precursor solutions used in non-vacuum growth methods for $CuInSe_2$ and $CuGaSe_2$ based photovoltaic cells. These growth methods make more efficient use of material, time, and energy than traditional vacuum methods. The formation energies of several carbon impurities are calculated using the hybrid HSE06 functional. C_{Cu} acts as a shallow donor, C_{In} and interstitial C yield deep donor levels in $CuInSe_2$, while in $CuGaSe_2$ C_{Ga} and interstitial C act as deep amphoteric defects. So, these defects reduce the majority carrier (hole) concentration in p-type $CuInSe_2$ and $CuGaSe_2$ by compensating the acceptor levels. The deep defects are likely to act as recombination centers for the photogenerated charge carriers and are thus detrimental for the performance of the photovoltaic cells. On the other hand, the formation energies of the carbon impurities are high, even under C-rich growth conditions. Thus, few C impurities will form in $CuInSe_2$ and $CuGaSe_2$ in thermodynamic equilibrium. However, the deposition of the precursor solution in non-vacuum growth methods presents conditions far from thermodynamic equilibrium. In this case, our calculations show that C impurities formed in non-equilibrium tend to segregate from $CuInSe_2$ and $CuGaSe_2$ by approaching thermodynamic equilibrium, e.g., via thorough annealing. © *2015 AIP Publishing LLC*.
[http://dx.doi.org/10.1063/1.4905538]

I. INTRODUCTION

$CuInSe_2$ (CIS) and $CuGaSe_2$ (CGS) are I-III-VI_2 semiconductors of the chalcopyrite family that form the semiconductor alloy $CuIn_{1-x}Ga_xSe_2$ (CIGS), where $0 \leq x \leq 1$. CIGS is of interest as absorber in photovoltaic cells, in particular thin-film photovoltaic cells, owing to its very high optical absorption coefficient.[1] Currently, the most common synthesis methods for polycrystalline CIGS layers can be divided into two categories: coevaporation and sequential deposition methods. Highly efficient CIGS thin-film photovoltaic cells, with efficiencies exceeding 20% both on glass substrates[2] and flexible substrates,[3] can be made through coevaporation of Cu, In, Ga, and Se in a vacuum chamber, using a three-stage process.[1,4] On the other hand, in sequential deposition methods, a precursor material is first prepared. The precursor is subsequently deposited on a substrate and annealed, inducing the chalcogenization reaction. Sequential methods are particularly suitable for the synthesis of large-area films.[4] The standard sequential method consists of preparing a precursor of Cu, In, and Ga by sputtering or thermal evaporation, both vacuum-based. In the next stage, called selenization, the precursor is exposed to Se while at the same time it is annealed at ~400–500 °C. Via a sequential process, for which the precursor has been sputtered, an efficiency of 20.9% has been achieved.[5] Coevaporation and the preparation of the precursor for the standard sequential method both involve vacuum conditions and are therefore afflicted with several problems. First of all, material losses of 20% to 50% are common.[1] The main cause is unintentional deposition of material on the vacuum chamber walls. Also, creating and maintaining a vacuum demands a high energy input. Furthermore, vacuum-based methods tend to be relatively slow. To overcome these limitations, non-vacuum-based sequential synthesis methods are gaining interest. These methods have been shown to reduce the material losses to almost zero.[6] They are also known as wet methods, as the precursor is usually included in a solution. Based on differences in the precursor material and deposition method, one distinguishes (i) coating through electrochemical reactions in a solution, (ii) coating with a molecular precursor solution by mechanical means, and (iii) particulate-based processes.[6] In the latter case, the particulates are solid nanoparticles, usually consisting of multiple oxide or selenide phases of Cu, In, and Ga, dispersed in an organic solvent. In this way, they form a sort of ink that is coated onto the substrate by printing, spraying, or spin coating. The organic solvents that have been reported in the scientific literature include a mixture of methanol and pyridine,[7] 1,5-pentanediol,[8] and a mixture of ethanol, terpineol, and ethyl cellulose.[9] In Ref. 9, the observed effect of the carbon stemming from the organic solvents is pointed out. It can form an amorphous layer between the CIGS layer and the Mo back contact, thus adding to the series resistance of the circuit. Moreover, residual carbon can be present in the entire film and is observed to limit the crystal growth. The authors try to minimize the presence of these carbon impurities by means of a three-step annealing process.

[a]Electronic mail: Jonas.Bekaert@uantwerpen.be

Currently, the main disadvantage of the non-vacuum, wet synthesis methods is the low efficiency of the resulting cells, usually below 10%.[6] To improve the efficiencies, the effect of impurities has to be elucidated, in particular carbon impurities, since carbon is abundantly present in the wet methods. Carbon impurities have been paid very little attention in previous first-principles studies. Therefore, we will address the important open question of what influence carbon-related point defects exert on the electric properties of CIGS. We have previously studied from first-principles how native point defects contribute to the conductivity in CIGS.[10] In this study, it was shown that the cation-related point defects, namely, the vacancy V_{Cu}, the vacancy $V_{In/Ga}$, and the antisite defect $Cu_{In/Ga}$ act as shallow acceptors, very likely giving rise to the three acceptor levels observed with photoluminescence, e.g., in Ref. 11. On the other hand, the shallow donor In/Ga_{Cu} is also abundantly present in samples grown under In/Ga-rich conditions. This donor compensates to a large extent the acceptor defects, resulting in potential fluctuations through the material, also observed in photoluminescence spectra.[11] Throughout this study, the hybrid HSE functional was used for a better account of the band gap compared with standard density functional theory.[12] The hybrid functional has also been used in defect studies in CIGS, e.g., by Oikkonen *et al.*[13] and Pohl and Albe.[14]

To elucidate the effect of C impurities in CIGS, we present calculations of several types of C impurities in CIS and CGS. More specifically, the structural and electronic properties of the substitutional defect C_{Cu} in CIS and CGS, the substitutional defects C_{In} and C_{Ga} in CIS and CGS, respectively, and the C interstitial (C_i) in both materials are discussed. The possibility to form a C interstitial can be understood in terms of the atomic radii. The C atom has a radius of ~0.77 Å (defined in the tetrahedral covalent bond),[15] which is small compared with the interatomic distances in CIS and CGS. To start with, the important concepts of a first-principles study of defects, such as the formation energy and transition levels, are reviewed. Subsequently, the deformation of the lattice by the C impurities and their electronic activity based on the formation energy of different possible charge states are discussed. In this way, we ultimately try to answer whether C impurities easily form in CIGS and what effect they produce on the performance of CIGS as a photovoltaic absorber material.

II. THEORETICAL METHOD TO STUDY C-RELATED POINT DEFECTS

A. Formation energy, defect concentration

In general, the formation energy of a defect $\mathcal{D}$ in charge state q, $E_f(\mathcal{D},q)$ is defined as[10,16,17]

$$E_f(\mathcal{D},q) = E_{tot}(\mathcal{D},q) - E_{tot}(\text{bulk}) + \sum_\nu n_\nu \mu_\nu + q(E_{VBM} + E_F + \Delta V^{(q)}). \quad (1)$$

In this expression, $E_{tot}(\mathcal{D},q)$ is the total energy of a supercell containing the defect and $E_{tot}(\text{bulk})$ is the total energy of the bulk supercell (i.e., without defect). In the third term, μ_ν are the chemical potentials of the atoms that are exchanged with external reservoirs to form the defect. The absolute values $|n_\nu|$ give the number of exchanged atoms of element ν; furthermore, if the atoms are added to the system $n_\nu < 0$, in case they are removed $n_\nu > 0$. For instance, for the C_{Cu} antisite defect this term is $\mu_{Cu} - \mu_C$. The chemical potentials represent the chemical conditions during the growth of the material. The chemical potential can be rewritten as the sum of the chemical potential of the elemental phase (μ_ν^{elem}) and a deviation $\Delta\mu_\nu$, where a more negative $\Delta\mu_\nu$ means ν-poorer growth conditions. The range of the $\Delta\mu_\nu$ of the atoms making up the host material (in this case CIS and CGS) is restricted in thermodynamic equilibrium (cf. Ref. 10). For charged defects, the last term in Eq. (1) describes the exchange of electrons with the electron reservoir at the Fermi level E_F, referenced to E_{VBM}, the top of the valence band of the bulk cell ($q < 0$ if they are added to the supercell and $q > 0$ if they are removed). Finally, $\Delta V^{(q)}$ is the difference in reference potential of the supercell without defect and with defect. It was demonstrated by Lyons *et al.* in a comparative study of correction schemes for the effect of the supercell size that the scheme based on $\Delta V^{(q)}$ is consistent with other schemes, e.g., the Madelung correction.[18] Equation (1) thus states that the formation energies of the defects are linear functions of E_F and this is how they are conveniently represented. The Fermi level at which the formation energies of different charge states q and q' of a certain defect become equal is called the transition level $\varepsilon(\mathcal{D},q/q')$. The transition levels relative to the valence and conduction band determine the electrical activity of the defect state. The concentration of defects of type $\mathcal{D}$ in charge state q in thermodynamic equilibrium follows a Boltzmann distribution:[16,19]

$$N(\mathcal{D},q) = M_\mathcal{D} g_q \exp\left[-E_f(\mathcal{D},q)/(k_B T)\right], \quad (2)$$

where $M_\mathcal{D}$ denotes the concentration of lattice sites where the defect can originate, for example, to form C_{Cu} in CIS the concentration of Cu lattice sites is $M_{C_{Cu}} = 1.13 \times 10^{22}$ cm^{-3}. g_q is an electronic degeneracy factor for charge state q, including spin degeneracy.[16]

B. Computational details

As mentioned in the Introduction, our calculations make use of a hybrid functional, more specifically the HSE06 functional implemented in the VASP code.[20,21] With the standard HSE06 functional, the exchange interaction is still overscreened, resulting in underestimated band gaps amounting to 0.85 eV for CIS and 1.37 eV for CGS. Therefore, the experimental band gaps of ~1.0 eV for CIS and ~1.7 eV for CGS correspond to an enhanced fraction of Hartree-Fock exchange.[1,22] We have determined that $\alpha = 0.2780$ for CIS and $\alpha = 0.3098$ for CGS produce realistic band gaps of 1.00 eV and 1.72 eV, respectively. We use the adapted HSE06 functional throughout this paper since correct values for the band gaps are crucial for the calculation of defect formation energies. Electron-ion interactions are treated using projector augmented wave (PAW) potentials, including Cu-$3d^{10}4s^1$, Ga-$3d^{10}4s^24p^1$, In-$4d^{10}5s^25p^1$, Se-$4s^24p^4$, and C-$2s^22p^2$ as valence electrons. The energy cutoff for the

plane-wave basis is set to 500 eV to achieve a convergence of the total energy of the cell within ~0.1 meV per atom. The C impurities are placed in a supercell of the primitive cell, to reduce electrostatic interactions between the impurities adding to the total energy. Previously, we have performed a convergence test for the supercell size for different charge states of the Cu vacancy in CIS, finding that the $2 \times 2 \times 2$ supercell of the primitive cell of CIGS, containing 64 atoms, yields well-converged values.[10] Based on this, the formation energies of the C impurities have also been calculated in 64-atom supercells. The atomic positions in these supercells are relaxed until all forces are smaller than 0.05 eV/Å, while keeping the cell shape and volume constant to avoid taking into account the effect of spurious elastic defect-defect interaction on the lattice parameters.[23] The charge state q of the impurity is simulated by adding $q = .., -2, -1, 0, +1, +2, ..$ electrons to the supercell. For integration over the Brillouin zone, a $2 \times 2 \times 2$ Γ-centered Monkhorst-Pack **k**-point grid is used. Finally, we calculate the correction for the reference potential $\Delta V^{(q)}$ in Eq. (1) via the method described in Ref. 17.

III. RESULTS AND DISCUSSION

A. Structural properties

CIS and CGS adopt the body-centered tetragonal chalcopyrite structure, characterized by space group $I\bar{4}2d$, in their ground state. The calculated lattice parameters (of the conventional cell) of pristine CIS are $a = 5.832$ Å, $c = 11.735$ Å, and anion displacement $u = 0.229$, and those of CGS are $a = 5.652$ Å, $c = 11.119$ Å, and $u = 0.253$. As we have already mentioned, the cell shape and volume are kept constant after introducing the C impurities. The ionic positions are relaxed, whereby mainly the interatomic distances of the C impurities and the surrounding atoms are affected. In Fig. 1, we present these distances as a function of the excess charge of the impurity, q. In Fig. 1(a), one can observe that the interatomic C_{Cu}-Se distance reaches a maximum for the neutral cell ($q = 0$) but is smaller than the unperturbed Cu-Se distance for all charge states. These observations hold in both CIS and CGS. The distances C_{In}-Se and C_{Ga}-Se, on the other hand, converge to maximal values of ~2.30 Å in CIS and ~2.27 Å in CGS for negative q. Similarly, for positive q the distances converge to minimal values of ~2.05 Å in CIS and CGS. Finally, the initial position of the C_i defect is chosen such that the distances to all other atoms in the lattice are maximal. An example of the structure after relaxation is shown in Fig. 2 for CIS in the $q = 0$ charge state. In fact, for $q = 0$ the distances between C_i and the first nearest neighbor $NN_1 = Se$ are almost equal in CIS and CGS; this also holds for the second nearest neighbor $NN_2 = Cu$. The distances C_i-Se in both CIS and CGS are overall linearly decreasing with increasing charge state, with the exception of $q = +2$ in host CGS. The distance C_i-NN_2 ($NN_2 = Cu$ except for $q < 0$ in host CGS, where $NN_2 = Ga$) reaches a minimum for $q = 0$. For positive charge states, this interatomic distance converges to ~2 Å in CIS and CGS. For the negative charge states, however, there is a strong increase

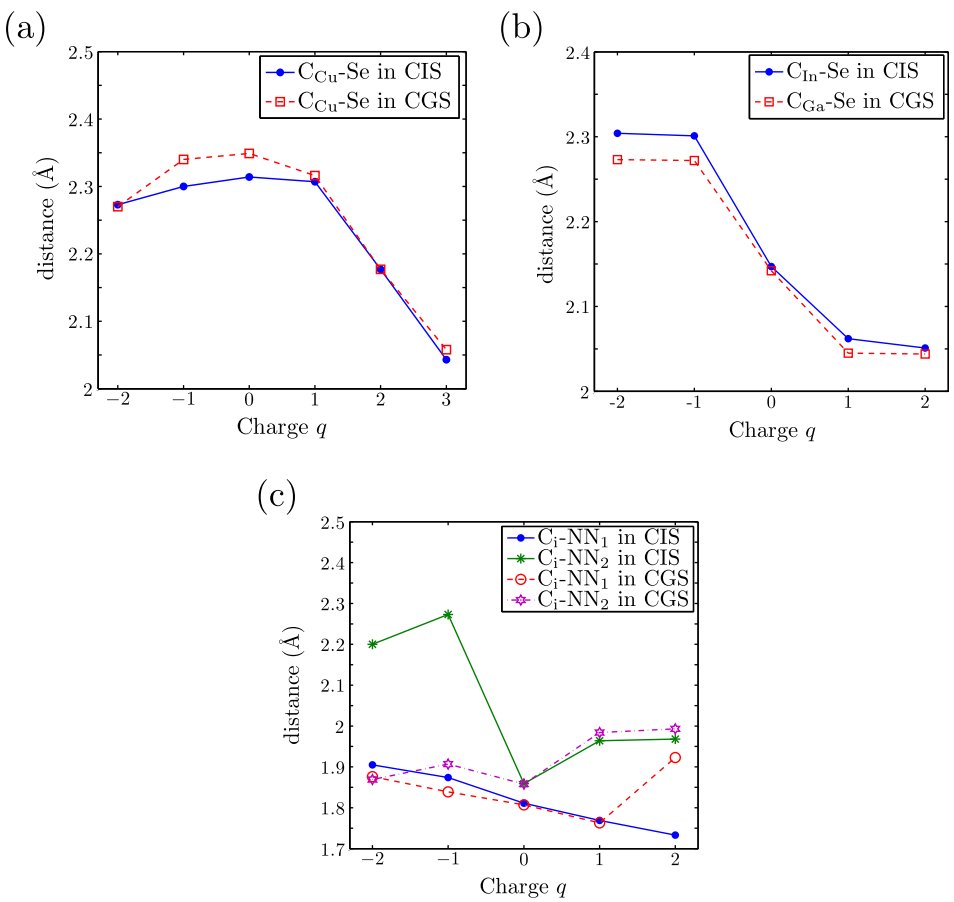

FIG. 1. The interatomic distances (Å) between the C impurities and the surrounding atoms as a function of the excess charge q of the impurity. The lines connecting the values for different charge states serve as a guide for the eye. In (a) the distance C_{Cu}-Se is given, in (b) the distances C_{In}-Se and C_{Ga}-Se and in (c) the distance between C_i and the two nearest neighbors (NN). These are $NN_1 = Se$ in both CIS and CGS for all charge states and $NN_2 = Cu$ except for $q = -1, -2$ in CGS where the second nearest neighbor is Ga. For comparison, the calculated unperturbed interatomic distances are $d(Cu - Se) = 2.456$ Å in CIS and $d(Cu - Se) = 2.440$ Å in CGS and $d(In - Se) = 2.609$ Å in CIS and $d(Ga - Se) = 2.429$ Å in CGS.

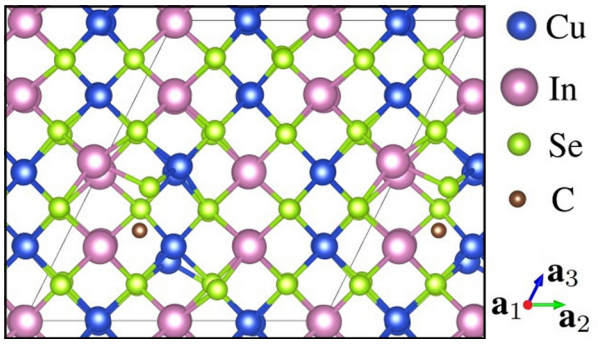

FIG. 2. The lattice distortion in CIS due to the C_i defect. The $2 \times 2 \times 2$ supercell is indicated by the gray lines. The position of the interstitial in terms of $\mathbf{a}_1 = (2a, 0, 0)$, $\mathbf{a}_2 = (0, 2a, 0)$ and $\mathbf{a}_3 = (a, a, c)$, the primitive lattice vectors that span the $2 \times 2 \times 2$ supercell, is $\sim(0.97, 0.23, 0.30)$.

to values exceeding 2.2 Å in CIS, whereas the C_i-Ga distance remains around 1.9 Å in CGS. In general, one can summarize that the lattice deformation due the substitutional C impurities are similar in CIS and CGS for all charge states, but that lattice deformations due to interstitial C are more complex. This complex behavior seems to be dominated by the excess charge states, since in the neutral case the interatomic distances are almost equal in CIS and CGS.

B. Electronic properties

The formation energies of the preferred charge states of the different C impurities are plotted as a function of the Fermi level E_F in Fig. 3, different chemical growth conditions being implemented via the chemical potentials of the exchanged atoms. The transitions between the charge states are however not affected by the chemical potentials, as follows from Eq. (1). The formation energies of C_{Cu} show that it prefers to donate electrons. For small E_F, the $q = +3$ charge state is favored owing to the 3 extra outer shell electrons of C compared with Cu. For higher E_F donating 3 electrons becomes too energetically expensive, resulting in a direct transition to the $q = +1$ charge state at 0.81 eV for CIS and a similar transition at 0.92 eV in CGS. These transition levels are also listed in Table I. Since the transition to the neutral charge states lies within the conduction band of the host material, C_{Cu} acts as a shallow donor in both CIS and CGS. Moreover, it can compensate the native acceptor-type defects in p-type CIGS, thereby reducing the free hole concentration. The substitutional defects C_{In} and C_{Ga} adopt the $q = +1$ charge state in the lower range of E_F. The interpretation is again clear: by donating one electron, C carries the same number of outer shell electrons as In and Ga. Then, with increasing E_F donating electrons becomes energetically unfavorable and C_{In} undergoes a $+1/0$ transition at $E_F = 0.74$ eV (0.26 eV from the CBM) in CIS. In CGS, there is a direct $+1/-1$ transition at $E_F = 1.38$ eV (0.34 eV from the CBM). Since C_{Ga} acts as both a deep acceptor and a deep donor, it is also called a deep amphoteric defect.[24] So, in p-type CIS and CGS, C_{In} and C_{Ga} give rise to deep donor levels, that compensate acceptor levels. As a result, they

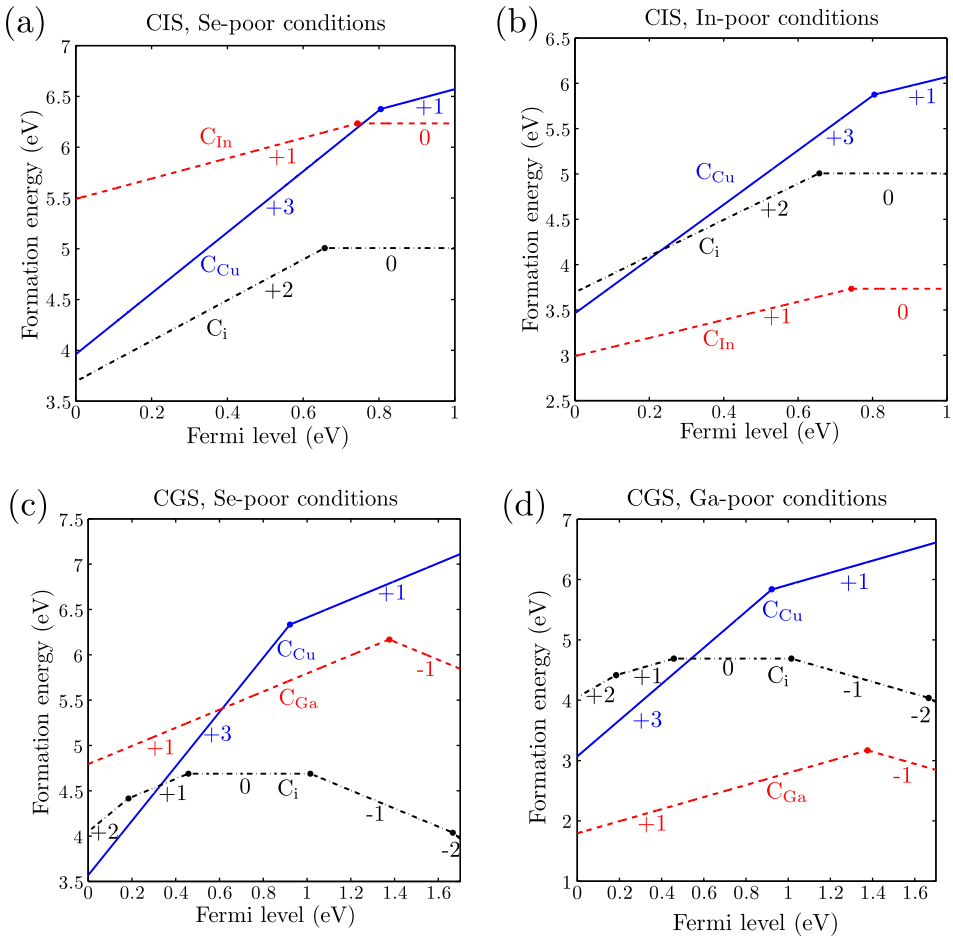

FIG. 3. Formation energies (eV) of preferred charge states of C_{Cu} (idem), C_{In} (C_{Ga}), and C_i (idem) in CIS (CGS), as a function of the Fermi level between VBM and CBM. The charge states are listed near the curves, while the transition levels are indicated by solid dots. Different growth conditions are compared, namely, Se-poor conditions, on one hand, and In/Ga-poor conditions, on the other hand. Here, we refer to the chemical potentials of these elements during growth, not to the composition of the compound which is grown. For CIS, we distinguish between (a) Se-poor conditions $(\Delta\mu_{Cu}, \Delta\mu_{In}) = (0, 0)$ eV and (b) In-poor conditions $(\Delta\mu_{Cu}, \Delta\mu_{In}) = (-0.5, -2.5)$ eV. Similarly, for CGS we compare (c) Se-poor conditions $(\Delta\mu_{Cu}, \Delta\mu_{Ga}) = (0, 0)$ eV with (d) Ga-poor conditions $(\Delta\mu_{Cu}, \Delta\mu_{Ga}) = (-0.5, -3.0)$ eV. In all cases, $\mu_C^{graphite}$ is used to calculate the exchange of C atoms.

TABLE I. Transition levels (eV) within the band gap, given w.r.t. the VBM.

Host	Defect	Transition q/q'	$\varepsilon(q/q')$ (eV)
CIS	C_{Cu}	+3/+1	0.81
CGS	C_{Cu}	+3/+1	0.92
CIS	C_{In}	+1/0	0.74
CGS	C_{Ga}	+1/−1	1.38
CIS	C_i	+2/0	0.66
CGS	C_i	+2/+1	0.18
CGS	C_i	+1/0	0.46
CGS	C_i	0/−1	1.02
CGS	C_i	−1/−2	1.67

become positively charged and subsequently they can trap photogenerated minority carriers (electrons). Since the transition levels of C_{In} and C_{Ga} lie deep within the gap, the trapped electron will likely recombine with a hole, rather than being re-emitted to the CBM.[25] Consequently, C_{In} and C_{Ga} can be expected to be recombination centers for the photogenerated charge carriers, instead of simple traps. C_i in CIS donates two electrons provided that $E_F < \varepsilon(+2/0) = 0.66$ eV (0.34 eV from the CBM), and therefore, C_i acts as a deep donor in CIS. In CGS, C_i also prefers to donate electrons within the lower range of E_F, while there is a transition from $q=+2$ to $q=+1$ at 0.18 eV. Subsequently, at 0.46 eV the neutral state becomes the preferred charge state and for even higher values of E_F, C_i favors acceptor-like behavior in CGS. The transition levels are $\varepsilon(0/-1) = 1.02$ eV and $\varepsilon(-1/-2) = 1.67$ eV, and therefore, C_i acts as a deep amphoteric defect in CGS. Thus, it is a deep level that traps either charge carrier type, depending on E_F. In p-type CIS and CGS, C_i can again compensate acceptor levels, thereby starting to trap photogenerated electrons. Moreover, since the transition level lies deep within the gap, C_i is likely to also trap photogenerated holes, thus acting as a recombination center. In summary, C impurities present in CIS and CGS are detrimental for the performance of p-type CIS and CGS in a photovoltaic device, since they act as shallow donors (C_{Cu}) or deep donors (C_{In}, C_{Ga}, and C_i). They compensate acceptor levels, so subsequently they can trap photogenerated minority carriers (electrons). Since the defect levels lie deep within the gap, they are also likely to trap majority carriers (holes), and therefore, act as recombination centers.

The concentration of C impurities that will form in thermodynamic equilibrium is a function of the formation energy according to the Boltzmann distribution in Eq. (2). The formation energy itself depends on the chemical growth conditions via the chemical potentials. In Fig. 3(a), the formation energies are calculated under Se-poor conditions. In this case, it has been demonstrated that E_F is pinned close to the CBM because the donor In_{Cu} has a low formation energy.[10] Under these conditions, the defect with the lowest formation energy is C_i, but its formation energy still amounts to ~5 eV in n-type CIS. Moreover, it is not electrically active for $0.66\,\text{eV} < E_F < 1.00$ eV. On the other hand, to obtain p-type conductivity through native point defects, more In-poor conditions are required, such as those leading to Fig. 3(b). In this case, owing to the In-poor conditions, C_{In} has become the dominant C impurity. The formation energy of this defect is ~3 eV if E_F is close to the VBM in p-type CIS. Using Eq. (2), this results in a very small concentration of C_{In} impurities in thermodynamic equilibrium. In Fig. 3(c), the formation energies of the C impurities in CGS grown under Se-poor conditions are displayed. Like in CIS, C_i is the impurity with the lowest formation energy under these conditions. Since the formation energy exceeds 3.5 eV, few impurities will form in thermodynamic equilibrium. Under Ga-poor conditions, the native defects pin E_F at the VBM, so based on the formation energies in Fig. 3(d) C_{Ga} is the dominant C impurity. Its formation energy is ~1.8 eV, so at a typical annealing temperature of 500 °C (cf. Refs. 8 and 9), assuming thermodynamic equilibrium, only $\sim 2.08 \times 10^{10}$ cm^{-3} C_{Ga} defects would form. This is negligible compared with the concentration of lattice sites where the defect could form ($M_{C_{Cu}} = 1.13 \times 10^{22}$ cm^{-3}).

In the results presented in Fig. 3, we had assumed that the reservoir for C atoms is the elemental solid, graphite. In reality, the C atoms are part of the organic molecules of the solution used to disperse the nanoparticle precursor. Methanol (CH_3OH) is probably the most simple organic solvent used in these solutions [7]. It can readily be studied using the hybrid functional, enclosing it in a box, i.e., a supercell with an edge of 30 Å that is otherwise empty. In order to calculate the formation energy of CH_3OH, the total energy of graphite is to be taken into account. The total energies of the O_2 and H_2 molecules have to be included as well. For this computation, O_2 and H_2 are enclosed in boxes with edges measuring 30 Å. The total energy of O_2 is obtained in a spin-polarized calculation, since the triplet state with two unpaired electrons forms the ground state. The calculated value of the heat of formation of methanol is thus (with $N_{atom} = 4$ in the graphite unit cell)

$$\begin{aligned}\Delta H_f(CH_3OH) &= E_{tot}(CH_3OH) - \frac{E_{tot}(\text{graphite})}{N_{atom}} \\ &\quad - \frac{1}{2}E_{tot}(O_2) - 2E_{tot}(H_2) \\ &= -2.71\,\text{eV}. \end{aligned} \tag{3}$$

An experimentally obtained value of the heat of formation in the liquid phase is −238.4 kJ/mol.[26] This corresponds to −2.47 eV per CH_3OH molecule, yielding a good agreement with the theoretical value. In order that the C atoms of CH_3OH do not precipitate into graphite, one requires that $\Delta\mu_C \leq 0$ eV. Consequently, the chemical potential μ_C ranges from μ_C^{graphite} under C-rich conditions to $\mu_C^{\text{graphite}} - 2.71$ eV under C-poor conditions. We find that the formation energies can shift upwards with +2.71 eV at most (under C-poor conditions, which are not plausible). Thus, we can conclude that a reservoir containing organic molecules leads to an increase of the formation energy of C impurities and therefore a decrease of the C impurity concentrations. A similar reasoning as for methanol applies for other possible organic solvents, while the increase of the formation energy is most significant for very stable compounds, with a low heat of

formation (per C atom included). This yields a practical guideline for the choice of organic solvent.

The Boltzmann distribution (Eq. (2)) predicts low C impurity concentrations in ideal thermodynamic equilibrium due to the high formation energy of the C impurities. However, non-vacuum growth methods are far from thermodynamic equilibrium during the initial stage—the deposition of the nanoparticle ink—since considerable flows of matter are required to transform the nanoparticle ink into a thin film. Therefore, a non-negligible concentration of C impurities could form in CIS and CGS, as observed in experiment, e.g., Refs. 8 and 9. Our calculations explain the experimental observation that a CIGS film initially doped with C can be made nearly C-free by long annealing in air.[9] Namely, the annealing establishes conditions near thermodynamic equilibrium, where we have shown C impurities have high formation energy and will therefore segregate to the surface of the CIGS film. Subsequently, the supplied air removes the C permanently, likely through the formation of CO_2. In Ref. 9, the authors report a C residue around the accuracy limit of their measurement ($\sim$3 at. %). From our calculations, one can draw the conclusion that the remaining C atoms are not likely to be present in the form of point defects, but rather in the form of a separate phase, e.g., C clusters. The first-principles results presented here are valid for bulk CIS and CGS, including grains, except at the grain boundaries. In addition, more experimental and theoretical work on C impurities, also at the grain boundaries, is required.

IV. CONCLUSION

We have studied C impurities in CIS and CGS, related to new non-vacuum growth methods using, e.g., nanoparticle inks. We have calculated the formation energies of several substitutional impurities and also an interstitial impurity using the hybrid functional HSE06. We found that C_{Cu} acts as a shallow donor in both CIS and CGS. C_{In} and interstitial C yield deep donor levels in CIS, while in CGS C_{Ga} and interstitial C act as deep amphoteric defects. Therefore, in p-type CIS and CGS, these impurities will compensate acceptor levels, thereby reducing the majority carrier concentration, and trap the minority carriers (electrons). Since the transition levels of these defects lie deep within the gap, they are likely to also trap holes, i.e., they act as recombination centers. As such, C impurities are detrimental to the performance of CIGS photovoltaic device. On the other hand, the formation energies of the carbon impurities are high, including under C-rich growth conditions. Thus, few C impurities would form in $CuInSe_2$ and $CuGaSe_2$ in ideal thermodynamic equilibrium. However, non-vacuum growth methods are far from thermodynamic equilibrium. In this case, our calculations show that C impurities formed during non-equilibrium tend to segregate from $CuInSe_2$ and $CuGaSe_2$ upon approaching thermodynamic equilibrium (experimentally achievable via a long annealing procedure[9]).

ACKNOWLEDGMENTS

We gratefully acknowledge financial support from the science fund FWO-Flanders through project G.0150.13. The computational resources and services used in this work were provided by the VSC (Flemish Supercomputer Center) and the CalcUA core facility of the University of Antwerp, funded by the University of Antwerp, the Hercules Foundation and the Flemish Government—Department EWI.

[1]S. R. Kodigala, *Cu(In,Ga)Se$_2$ Based Thin Film Solar Cells* (Academic Press, 2010), p. 29.
[2]P. Jackson, D. Hariskos, E. Lotter, S. Paetel, R. Wuerz, R. Menner, W. Wischmann, and M. Powalla, Prog. Photovolt. Res. Appl. **19**, 894–897 (2011).
[3]A. Chirilă, P. Reinhard, F. Pianezzi, P. Bloesch, A. R. Uhl, C. Fella, L. Kranz, D. Keller, C. Gretener, H. Hagendorfer, D. Jaeger, R. Erni, S. Nishiwaki, S. Buecheler, and A. N. Tiwari, Nat. Mater. **12**, 1107–1111 (2013).
[4]U. P. Singh and S. P. Patra, Int. J. Photoenergy **2010**, 468147 (2010).
[5]M. Nakamura, N. Yoneyama, K. Horiguchi, Y. Iwata, K. Yamaguchi, H. Sugimoto, and T. Kato, in *IEEE 40th Photovoltaic Specialists Conference*, 2014, pp. 0107–0110.
[6]C. J. Hibberd, E. Chassaing, W. Liu, D. B. Mitzi, D. Lincot, and A. N. Tiwari, Prog. Photovolt.: Res. Appl. **18**, 434–452 (2010).
[7]D. L. Schulz, C. J. Curtis, R. A. Flitton, H. Wiesner, J. Keane, R. J. Matson, J. D. Perkins, and D. S. Ginley, J. Electron. Mater. **27**, 433 (1998).
[8]A. E. Zaghi, M. Buffière, G. Brammertz, M. Batuk, N. Lenaers, B. Kniknie, J. Hadermann, M. Meuris, J. Poortmans, and J. Vleugels, Adv. Powder Technol. **25**, 1254–1261 (2014).
[9]E. Lee, S. J. Park, J. W. Cho, J. Gwak, M.-K. Oh, and B. K. Min, Sol. Energy Mater. Sol. Cells **95**, 2928–2932 (2011).
[10]J. Bekaert, R. Saniz, B. Partoens, and D. Lamoen, Phys. Chem. Chem. Phys. **16**, 22299–22308 (2014).
[11]S. Siebentritt, L. Gütay, D. Regesch, Y. Aida, and V. Deprédurand, Sol. Energy Mater. Sol. Cells **119**, 18–25 (2013).
[12]J. Heyd, G. E. Scuseria, and M. Ernzerhof, J. Chem. Phys. **118**, 8207–8215 (2003).
[13]L. E. Oikkonen, M. G. Ganchenkova, A. P. Seitsonen, and R. M. Nieminen, Phys. Rev. B **86**, 165115 (2012).
[14]J. Pohl and K. Albe, Phys. Rev. B **87**, 245203 (2013).
[15]C. Kittel, *Introduction to Solid State Physics*, 8th ed. (John Wiley & Sons, 2005), p. 71.
[16]J. Ma, S.-H. Wei, T. A. Gessert, and K. K. Chin, Phys. Rev. B **83**, 245207 (2011).
[17]M. N. Amini, R. Saniz, D. Lamoen, and B. Partoens, J. Appl. Phys. **110**, 063521 (2011).
[18]J. L. Lyons, A. Janotti, and C. G. Van de Walle, Phys. Rev. Lett. **108**, 156403 (2012).
[19]C. G. Van de Walle, D. B. Laks, G. F. Neumark, and S. T. Pantelides, Phys. Rev. B **47**, 9425–9434 (1993).
[20]G. Kresse and J. Furthmüller, Comput. Mater. Sci. **6**, 15–20 (1996).
[21]J. Paier, M. Marsman, K. Hummer, and G. Kresse, J. Chem. Phys. **124**, 154709 (2006).
[22]T. Tinoco, C. Rincón, M. Quintero, and G. Sánchez Pérez, Phys. Status Solidi A **124**, 427 (1991).
[23]C. G. Van de Walle and J. Neugebauer, J. Appl. Phys. **95**, 3851–3879 (2004).
[24]C. Freysoldt, B. Grabowski, T. Hickel, J. Neugebauer, G. Kresse, A. Janotti, and C. G. Van de Walle, Rev. Mod. Phys. **86**, 253–305 (2014).
[25]R. Scheer and H.-W. Schock, *Chalcogenide Photovoltaics*, 1st ed. (Wiley-VCH, 2011), pp. 44–50.
[26]See http://webbook.nist.gov/cgi/cbook.cgi?ID=C67561 for NIST, "Methyl alcohol," (last accessed July 2014).